Extracting Instantons from the Lattice

Falk Zimmermann*

Helmholtz Institute for Radiation and Nuclear Physics, University of Bonn
Nußallee 14-16, 53115 Bonn, Germany

E-mail: fzimmermann@hiskp.uni-bonn.de

In this talk, I summarize phenomenological results on topology, in particular the extraction of distinct topological sectors that resemble instantons, and support the picture of the QCD vacuum being filled with highly localized topological excitations. Combining the identification of topological sectors (connected regions of either left- or right-handed winding in $n_f = 2 + 1 + 1$ configurations [1]) with a simple charge gradient approach increases the number of instanton sectors found. Such sectors deviate from the background by a distinct charge-volume behaviour and, in addition, by a high degree of self-duality. Defining the topological charge density with an improved $O(a^6)$ field strength removes leading UV lattice artefacts that would otherwise contribute to the multiplicative renormalization constant. As a result, we find that the total charge of the configurations Q is very close to integers and the charge content of the instanton sectors is close to ± 1.

In addition, I show that the topological charge density contains a wave standing in the simulation box and present evidence for a physical phenomenon as well as hints in favour of a link to the (auto)correlation oscillations introduced by the HMC [2].

The 40th International Symposium on Lattice Field Theory (Lattice 2023)
July 31st - August 4th, 2023
Fermi National Accelerator Laboratory

---

*Speaker
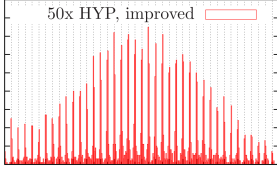
(a) B55.32 the Q histogram aligns well with integer numbers (grid)
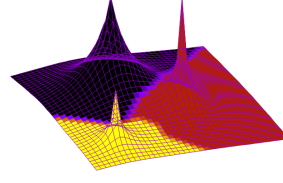
(b) Extraction of topological sectors defined by the gradients of composite fields such as $q(x) \cdot z(x)$.

Excitations of the gauge field have been a less popular to field to study in comparison to excitations made from quarks. This may be attributed to hadrons being more accessible via accelerator experiments and the gauge field being only probed indirectly via fermionic processes.

In the elusive zoo of gauge field excitations, the pseudoscalar channel houses one of the most prominent states, the family of classical instanton solutions which represent complete (integer) windings of the gauge field. Instanton solutions appear to be strongly localised, which depending on the gauge either corresponds to a $1/r$ (regular gauge) or $1/r^3$ slope (singular gauge) of the gauge field. Instantons are associated with chiral symmetry breaking and quark confinement. Recent theoretical advances suggest sizeable contributions to interquark forces in mesons [3] as well promising possibilities for experimental verification. They are considered on of last predictions of the standard model needing experimental verification and here are increasing efforts to find instanton signatures at the LHC [4],[5].

The experiments will benefit from a profound knowledge of topological excitations and their associated degrees of freedom. An instanton splitting into two increasingly separated merons will span an even larger affected distance and is therefore expected [6] to contribute significantly to to the area law of the static quark-antiquark potential associated with quark confinement. In this paper we may have found some early evidence for merons on the lattice.

0.1 Setup: ensemble & definition of the topological charge

We evaluate the topological charge of a twisted mass ensemble (B55.32, $L = 32$, $T = 64$) with $N_f = 2 + 1 + 1$ and $m_\pi = 373$ MeV [7],[1]. The total charge per configuration has been computed for 5000 configurations; topological sectors have been extracted together with their charge content and volume (number of occupied lattice sites) for approximately 700 configurations and there is a high-detail data set of sectors (additional quantities such as boundary insecurities and self-duality) consisting of 250 configurations.

In order to study topological excitations, which are minima of the gauge action and go along with strongly localised amounts of the topological charges (*pseudoparticles*) the gluonic definition of the topology is to be preferred over fermionic counterparts. While the latter links topological phenomena via the index theorem, the gluonic definition

$$q(x) \equiv \frac{g^2}{32} \text{tr}[F_{\mu\nu}\widetilde{F}_{\mu\nu}], \quad F_{\mu\nu} \text{ field strength tensor} \tag{1}$$

is mathematically equivalent to the winding density of the gauge field. It thus provides the most direct access to local excitations as well as global features such as the homotopy classes of the gauge field. The disadvantage is the need to control UV divergences, which is usually achieved by

systematic cooling using the Yang-Mills gradient flow. In this work, we rely on the older 4D HYP smearing approach and note that the number of smearing iterations can be identified with a gradient flow time [8]. Cooling/smearing is known to diffuse pseudoparticles and different features appear at different scales, which is addressed by varying the step number N_{HYP}. We find that global charges to require a higher amount of smoothing (N_{HYP}=50) than local features such as meron sectors with $Q_{\text{sec}} \approx 0.5$. Traces can be found with $N_{\text{HYP}} = 10$ but not with $N_{\text{HYP}} = 50$. For this one task, HYP smearing may be preferable over the gradient flow which potentially collapses dimerons into instantons (and annihilates instanton-anti-instanton pairs) on smaller scales due to its similarity to cooling.

Our gluonic definition of the topological charge makes use of an highly improved version of the field strength tensor [9, 10]:

$$a^2 F_{\mu\nu} \equiv a^2 \left(1.5 \, \square_{\mu\nu}^{(1\times1)} - 0.15 \, \square_{\mu\nu}^{(2\times2)} - \frac{1}{90} \, \square_{\mu\nu}^{(3\times3)} + O(a^4) \right) \tag{2}$$

$$\text{with} \quad \square_{\mu\nu}^{(n\times n)} \equiv C_{\mu\nu}^{(n\times n)} - C_{\mu\nu}^{(n\times n)\dagger} - \frac{1}{3} \text{Tr} \left[C_{\mu\nu}^{(n\times n)} - C_{\mu\nu}^{(n\times n)\dagger} \right]$$

Here, $C_{\mu\nu}^{(n\times n)}$ represents the clover average of four $n \times n$ Wilson loops in the $\mu\nu$-plane. Inserting this $O(a^4)$ improved version of the field strength into the traditional field-theoretic definition of the topological charge gives

$$\rightarrow \quad a^4 q(x) = a^4 \left(\frac{g^2}{32} \epsilon_{\mu\nu\rho\sigma} \text{Tr} \left[F_{\mu\nu} F_{\rho\sigma} \right] + O(a^4) \right) . \tag{3}$$

Usually, the lattice density $q(x)$ requires a multiplicative $Z(\beta)$ renormalisation even after smearing away the UV divergences, in order to achieve $Q^{\text{conf}} \equiv a^4 \sum_{x \in V} q(x) \in \mathbb{Z}$. Surprisingly, the computing of the total charge for our twisted mass configurations via (3) already yields a spectrum of almost perfect integers ($N_{\text{Hyp}} = 50$), as can be seen in fig. 1a. Note that the $O(a^4)$ improvement of the sum (2) was a necessity, and a single clover average requires a multiplicative renormalisation constant even if the $O(a^2)$ UV divergences [11] are suppressed by the large number of $N_{HYP} = 50$ smearing steps.

0.1.1 Instantons & (Di-)Merons

Instantons and dimerons are both classical solutions of the YM equations of motion, corresponding to a full winding of the gauge field. Apart from the fact, that superpositions are no longer a classical solution, the dilute instanton gas model is often used to characterise the YM vacuum. Recently, a lattice study has found that instantons are more numerous and promotes the instanton liquid picture [12]. Most readers will be familiar with instantons, so we will only introduce dimerons: these pseudoparticles are basically an instanton split into two equal parts - despite the non-linear nature of the YM EOM, a spatially separated pair of merons remains a classical solution. Each constituent carries half of the topological charge. They are described by the gauge field:

$$A_\mu^{\text{DM}}(x; \{x_0, d, u, \rho = 0\}) = \left[\frac{(x - x_0 + d/2)_\nu}{(x - x_0 + d/2)^2 + \rho^2} + \frac{(x + x_0 - d/2)_\nu}{(x + x_0 - d/2) + \rho^2} \right] u^\dagger \Sigma_{\mu\nu} u$$

Whereas the 3-tensor $\Sigma_{\mu\nu} \equiv \eta_{a\mu\nu}\sigma_a$ can be expressed via the t'Hooft symbol $\eta_{a\mu\nu}$ and Pauli matrices σ_a. The parameter pack of the dimeron solution consists of the central position x_0, the vector d defining the orientation and length of the separation of the two meron peaks and u which is a $SU(2)$ matrix (embedded in $SU(3)$ for QCD) defining the orientation in colour space. To emphasise that the dimeron solution lacks the size parameter of the instanton solution, the parameter pack includes $\rho = 0$. The dimeron becomes an instanton in the limes $A_\mu^{\text{Inst}}(x; \{x_0, d, u, \rho\}) = \lim_{|d|\to 0} A_\mu^{\text{DM}}(x; \{x_0, d, u, \rho\})$, thereby re-enabling the size $\rho > 0$. The exchange of the 4-vector parameter d for the scalar size in this limit suggests that dimerons have a larger measure in the QCD path integral than instantons.

$$\lim_{|x|\to\infty} A_\mu^{\text{DM}}(x) = \lim_{|x|\to\infty} A_\mu^{\text{Inst}}(x) \rightarrow 2\frac{x_\nu}{x^2}\Sigma_{\mu\nu} \propto \frac{1}{||x||} \tag{4}$$

The long-distance behaviour can be altered via the (large) "singular" gauge transformation $\hat{U}(\hat{x}) \equiv i\hat{x}_\mu \sigma_\mu^{(+)}$ with $\sigma^{(+)} \equiv (\vec{\sigma}, i \cdot \mathbb{1})_\mu$, $\hat{x}_\mu \equiv x_\mu/\sqrt{x_\nu x_\nu}$:

$$A_\mu^{\text{sing DM}} \equiv \hat{U}^\dagger(\hat{x})A^{\text{DM}}\hat{U}(\hat{x}) + i\hat{U}^\dagger(\hat{x})\partial_\mu\hat{U}(\hat{x}) \implies \lim_{|x|\to\infty} A_\mu^{\text{sing DM}}(x) \propto \frac{1}{||x||^3} \tag{5}$$

Instantons transformed into the singular gauge and obtain the same steeper x^{-3} decay and separating a pair of merons far enough may make them effectively independent. Single merons are not a classical solution, cannot be transformed into the singular gauge individually and thus regain their x^{-1} behaviour for large d. Adding dimerons and the singular gauge to the picture opens up many possibilities for models of topological pseudoparticle liquids to deviate from the spatial decay behaviour of the usual BPST-instantons in the regular gauge and may be worthwhile when studying topological excitations on the lattice. In the following we show, that there is already some evidence for merons on the lattice by searching for topological sectors with $|Q| \approx 1/2$.

1. Extracting topological sectors: The gradient approach & the shark fin signal

Once the topological charge density $q(x)$ of a configuration has been computed via (3) one may define topological sectors by introducing a cutoff c: Then two lattice sites belong to the same sector if there is at least one continuous path between the two sites along which $q(x)$ never changes sign and $|q(x)| > c$ always holds. A small value for c is easy to find: if c becomes too small, the resulting number of sectors grows exponentially (we used $c = 0.0001$.) This approach would already be sufficient to find a signature of instantons: if sectors with charge content Q and volume V (number of lattice sites) are depicted in a $|Q|,V$-plot, one would notice a ray consisting of sectors roughly satisfying $|Q| \propto V$ and representing only noise. However there is a bifurcation from this line towards smaller V and $|Q| \lessapprox 1$. Such behaviour is shown in fig 2. However, with the naive algorithm the plot would continue periodically, so that there would also be a branch to $|Q| \lessapprox 2$, $|Q| \lessapprox 3$, ...

These repetitions correspond to sectors containing more than one instanton. They can be broken up by adding the rule that a new site can only be assigned to an existing sector if there is another site in the immediate neighbourhood that already belongs to the sector and has a higher value of $|q(x)|$. Now, sectors can only grown down the gradient. All topology extrema become seed sectors and the sectors must be grown in turn in order distribute the area evenly.
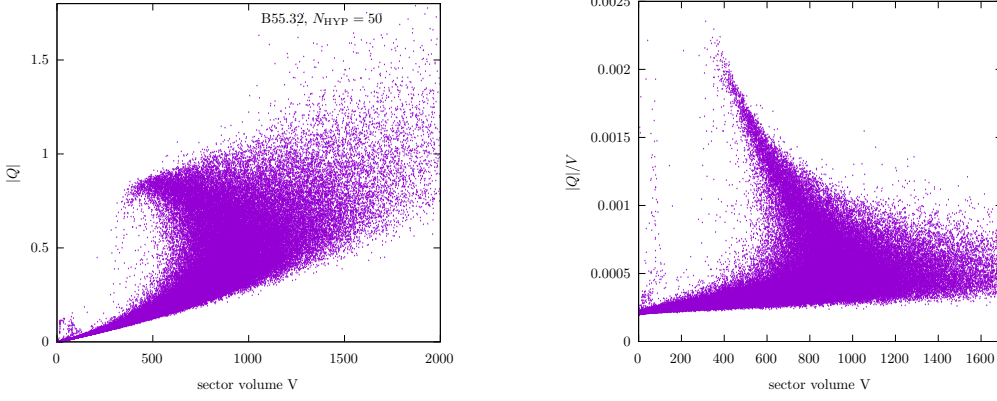
Figure 2: LHS: Topological sectors in the $(|Q|, V)$**-plane:** the dots near the origin correspond to sectors representing random fluctuations of the field $q(x)$. Sectors branching towards content $|Q| \approx 1$ start to approximate instantons. They contain points which are on average more (anti-)selfdual.

RHS: The plot on the LHS suffers from noise which adds a correlated $|Q_n| \propto V_n$ contribution to the sectors. This contribution can be reduced by considering Q/V and results in a sharper branch. Note that [8] independently found a similar behaviour in a quenched ensemble but with Q replaced by the sector extrema. They relate the observed graph to the shape of the BPST instantons.

(a) $\theta = q(x)z(x)$ **(b)** $\theta = q(x)z(x) \cdot \text{sign}(q(x))$ **(c)** $\theta = q(x)z(x)$, redistributed
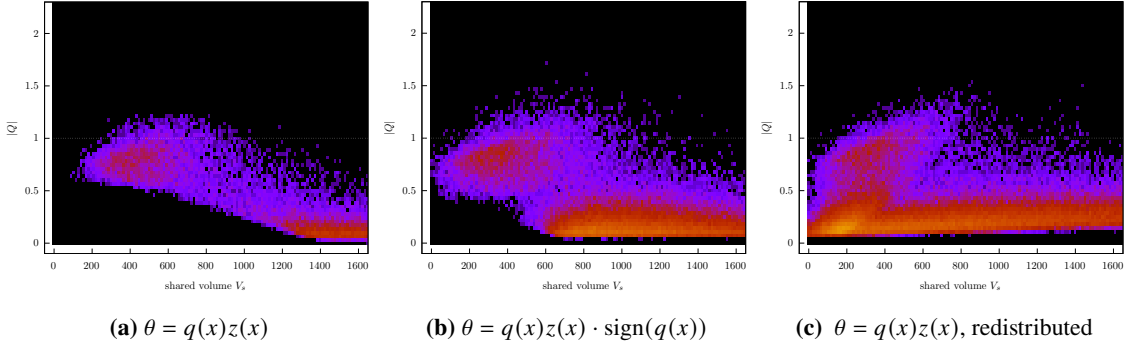
Figure 3: Sector densities in the $(|Q|, V)$**-plane** with $N_{\text{HYP}} = 10$: The extraction of instanton-like sectors includes the removal of unlikely candidates: low self-duality $|z| < 0.25$ and a small size $V < 200$ indicate noise. Similarity to instanton-like sectors was used to remove further sectors: the noise at the origin was suppressed (but for sectors with redistributed content). Now, there are two main heaps separated by the line $|Q| = 1/2$.

2. Multiple approaches to improved sectors & filtering via non-linear data correlation

To improve the signal, the topological density $q(x)$ can be replaced by a composite scalar field $\gamma(x)$:

$$\gamma(x) \in \{ q(x)z(x), q(x)z(x) \cdot \text{sign}(q(x)), q(x) \} \tag{6}$$

The field $z(A_\mu, x) \to [-1, 1]$ measures the selfduality: selfdual fields $F_{\mu\nu} = \tilde{F}_{\mu\nu} \Leftrightarrow z = 1$ are the hallmark of the instanton solution (and anti-selfdual fields $F_{\mu\nu} = -\tilde{F}_{\mu\nu} \Leftrightarrow z = -1$ the one of anti-instantons.) Then $\gamma(x) = q(x)z(x) \gtrless 0$ follows. This seems to be inconvenient, because now instanton and anti-instanton sectors are no longer divided by $|q(x)| < c$, can overlap and even

5

N_{HYP}	10		50	
γ	qz	$qz \cdot \text{sign}(q)$	qz	$qz \cdot \text{sign}(q)$
$q_c = 0.5$	100.2	123.3	56.1	62.0
$q_c = 0.7$	53.0	67.3	33.4	36.1

Table 1: Rough estimate of the number of pseudoparticles per configuration
A cutoff q_c was used to distinguish between noise and pseudoparticles. The values result in densities between $0.43\,\text{fm}^{-4}$ ($N_{\text{HYP}} = 50$, $\gamma = qz$, $q_c = 0.7$) and $1.6\,\text{fm}^{-4}$ ($N_{\text{HYP}} = 10$, $\gamma = qz \cdot \text{sign}(q)$, $q_c = 0.5$), which is in line with traditional estimates but an order of magnitude lower than the results in [12].

occur in the same sector. This can be avoided by switching to the field $\gamma = q(x)z(x) \cdot \text{sign}(q(x))$. However, the noise contributions Q_n to the sectors extracted from $q(x)z(x)$ are free to have any sign and thus cancel each other out to some extent and are the better choice in practice. Another attempt to improve the quality of the sector content is to account for sites, that could have belonged to several sectors. The associated size and charge content can then be redistributed equally between those sectors. (However this also turns out to add noise to relevant sectors - see fig 3.)

Besides the topological charge and V we keep track of a list of other sector properties. These include: the action S, the average selfduality $\bar{z}$ and derived quantities: the exclusive (non-shared) values Q_e, V_e, S_e, $\bar{z}_e$; the shared and redistributed amounts δQ, δV, δS, $\delta \bar{z}$.

The extraction of instanton-like sectors involves removing unlikely candidates: low selfduality $|z| < 0.25$ and a small size $V < 200$ indicate noise. Even for the short list above of sector features manual cutoffs become difficult. Since we were interested in merons, the idea now is to filter for them by selecting all instanton-like sectors via $0.75 < |Q| < 1.25$ and to compute a 2σ environment from these sectors for all features except Q and V. By assuming that merons are similar to instantons with respect to the other features, we exclude from the further analysis all sectors that do not match the 2σ environments. The process involves the computing of all the correlations between all the features from sectors within $0.75 < |Q| < 1.25$ and subsequentially removing the correlation[1]. Eventually, we can again study the distribution of the remaining sectors in the $(|Q|, V)$-plane: in the heat maps fig. 3 there are two main heaps respectively, separated by the line $|Q| = 1/2$. Obviously there is no meron heap, though. The best-case scenario is that meron and instanton signatures are mixed, here. In fact, the lower $|Q|$-boundary for sectors used to compute the correlation can be lowered to 0.5 with little effect on the overall analysis, but a further reduction drastically reduces the ability to remove noise sectors. The plots shown in this proceeding are based on a lower $|Q|$-boundary of 0.5 for improved statistics unless otherwise stated.

---

[1]If there is some non-local correlation, then excluding sectors incompatible with the 2σ environment would simply amount to removing all sectors except those in $0.75 < |Q| < 1.25$. Limiting the computation of the correlation to the instanton-like sectors prevents the noise sectors from introducing their correlation into the rest of the data set.
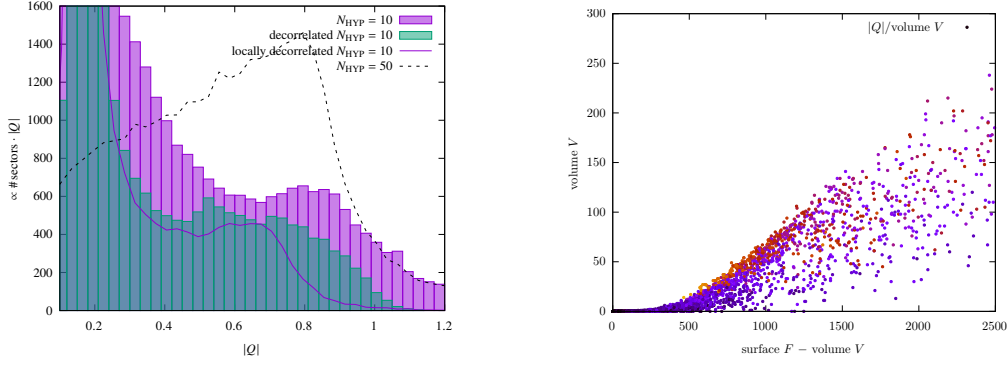
Figure 4: LHS: Q histograms: The magenta histogram represents sectors extracted from $\gamma = q(x)z(x)$. Note that there is peak at $Q \approx 0.8$. This peak can be associated with instantons and is a fairly typical/stable sight in this analysis. The peak could be raised/narrowed by rotating sectors in the $(|Q|, V)$-plane until the noise becomes roughly parallel to the x-axis in fig. 2, thereby removing the effect of noise on the (rotated) $|Q|$, but at the cost of having to rescale $|Q|$. The bold magenta line results from removing the $|Q|, V$-correlation as described in the text.

If the correlation removal is not restricted to the correlation found for instanton-like sectors, the **green histogram** follows: Here the removed correlation was dominated by the large number of noise sectors. The histogram has been rescaled back to $|Q| \approx 1$. No sectors were filtered out in this procedure. But there are some simple cutoffs that limit the accepted shared size($\delta V < 1800,\ 3200 \cdot |Q| > \delta V$). The result is a peak at $|Q| = 1/2$. If this corresponds to merons, the size restrictions may have been necessary to remove noisy dimerons that have not separated far enough.

The black line depicts the histogram of the larger data set (700 configurations) with $N_{\text{HYP}} = 50$: there is a strong signal for instantons. The instanton peaks in the histograms are to be expected to be located below $|Q| = 1$ due to the cutoff c and partial annihilation with surrounding sectors.

RHS: the sectors are surface-like! The number of sites being located on the 4D boundary of the sectors is only marginally smaller than the volume V. Sectors with high topological densities (red) are more likely to resemble instantons. Their volume tends to be larger, as expected for the spherical instanton solution.

3. Some results: the signal for localised instantons and merons

Strong signals for instantons can be seen in the history-representation of the $|Q|$-content of the sectors. See fig. 4 for the details. The same plot includes a $|Q|$-histogram with a small peak at $|Q| \approx 1/2$. This has been achieved by removing the correlation between size V and topological charge (which can be seen/estimated from the noise sectors in the $|Q|, V$-plot 2) from Q. However, this comes at the cost of Q needing to be rescaled, which can be done by making the histogram span the interval $|Q| \in [0, 1]$ again.

There are other ways to produce similar meron peaks, but the above mentioned is one of the simplest. Another possibility is to associate a continuous density with the sector data set by replacing the data points with normal distributions. There will then be higher densities in regions corresponding to classical topological excitations. Large gradients are an additional indication that the sector properties are favoured by being close to a classical solution. The details of this analysis can be found in fig. 5. The gradients do indeed indicate an additional topological state at $|Q| = 1/2$. Moreover, there seem to be traces of the transformation paths between such states.
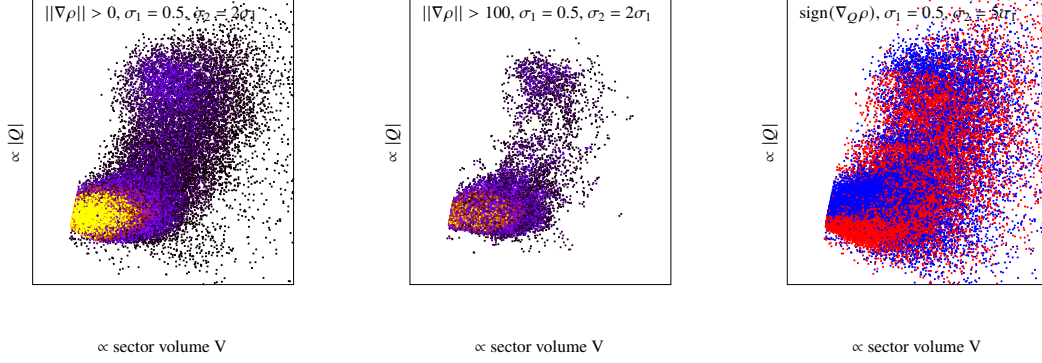
Figure 5: Selected densities of sectors shown in the $(|Q|, V)$-plane: The three plots show the density ρ of the same sector data set ($\gamma = qz$-sectors, correlation removed) and indicate the presence of merons. The density has been defined by associating each data point (sector) with a normal distribution with variance σ_1^2. A second, broader normal distribution (σ_2) is subtracted to counteract long-range contributions. Resulting densities are expressed via data point colours in the LHS and middle plots: At the bottom of all plots lies the high density area of the noise sectors, which is characterised by low $|Q| \approx 0$ content & small size. At the top is the accumulation area of instantons ($Q \approx 1$ - the scale of Q was lost when correlation was removed.)

The idea now is that some sector regions are favoured by QCD, for example by being close to classical solutions, and are marked by high density and large gradients of that density.

The sign of the $\partial_Q \rho$-component is plotted on the RHS: The two high density regions (bottom noise and instantons) are characterised by two successive horizontal layers of increasing (red) and falling ρ (blue). There is a third but less pronounced sign change of $\delta_Q \rho$ in the middle, at the estimated $|Q| = 0.5$ line, which indicates merons.

Restricting the density (**plotted centre**, 4D density ρ for $(|Q|, V, S, \delta V)$) to values > 100 helps to visualise an accumulation in the shape of a "mirrored S" which seems to connect the noise peak, merons and instantons.

4. Harmonic autocorrelation oscillations: the interplay with topology

Recently, there has been evidence for two topological phenomena: the first is crystals ([6, 13, 14], and the second is complex autocorrelation oscillations. The latter AC oscillations appear as harmonic oscillations in the MC time τ (configuration number). In addition, they manifest themselves as chequerboard-like standing wave patterns in the space-time and appear for various observables, especially pseudoscalars. The AC oscillations are probably linked to the canonical momenta introduced by the Molecular Dynamics step and a potential provided by the Lagrangian. The oscillations are hidden by short-time autocorrelations, but can be revealed by smoothing the affected physical correlators in the MC time. Both phenomena (topological crystals and AC waves) can be confused. Due to text length limitations, I will only list the main findings and refer to the figures 6,7a for the evidence:

- There is some evidence for topological excitations of opposite charge screening each other[6, 12], which can lead to the formation of the crystals.

- 1.) The AC oscillations appear as standing waves with respect to the time-like argument t for a lattice operator $\hat{o}$:

$$fc(\tau, t; \lambda) = \langle \hat{o}(t_0, \tau_0)\hat{o}(t_0 + t, \tau_0)\, \hat{o}(t_0, \tau_0 + \tau)\hat{o}(t_0 + t, \tau_0 + \tau)e^{-(\tau - \tau_0)^2/2\lambda^2}/\sqrt{2\pi\lambda^2}\rangle_{t_0, \tau_0}$$

- 2.) I could not find any waves for the usual topological correlator $\langle q(t_0)q(t_0 + t)\rangle_{t_0}$. This changes if there is no t_0-averaging ($t_0 = 0$) and if the topological charge densities are smoothed with respect to τ.
- The ensemble studied has twisted boundary conditions, resulting in lower wave signals when the correlator wraps around the boundary. The presence of a spatial analogue has not yet been investigated.
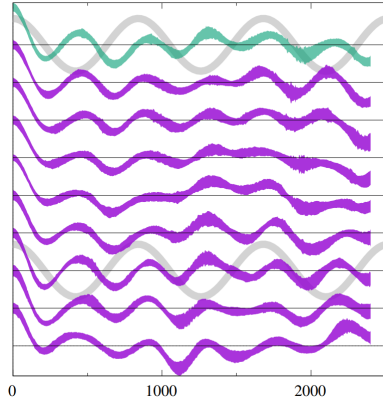
(a) B55.32 AC oscillations of the topological charge: Each horizontal line represents the abscissa for a time slice, the bottom one representing $t = 0$ and top-most magenta one representing $t = T − 1$. The green graph represents the time average. The gray line symbolises the AC oscillations of the pseudoscalar light meson correlator, which is the among the most affected. See [2] for details.
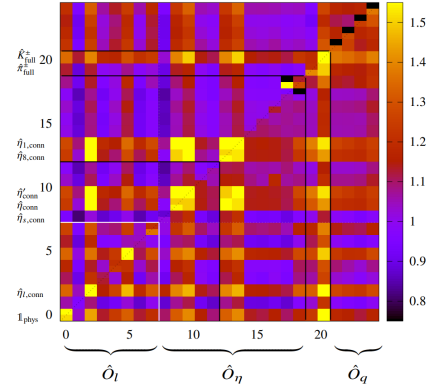
(b) A matrix showing how strongly lattice operators appear to be affected by AC oscillations. These matrix elements could be defined by integrating the absolute autocorrelation function.

Figure 6
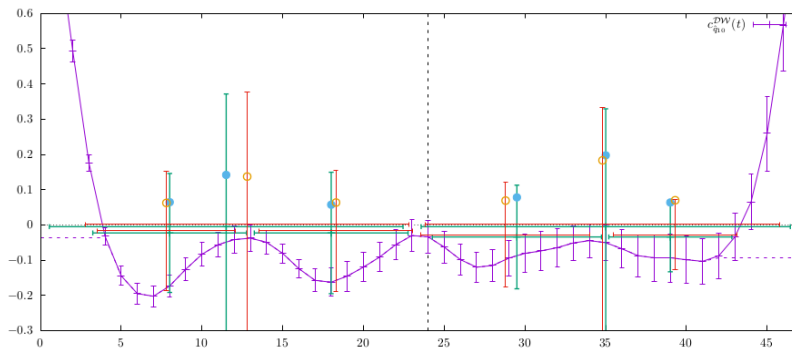
(a) A40.24: the topological wave correlator that appears when the reference time is fixed to the boundary ($t_0 = 0$ as described in 2.), $N_{\mathrm{HYP}} = 10$). The crosses are numerical estimates of the wave troughs. The horizontal extension indicates the width, the vertical the integrated depth and the points on the bars the standard deviation. These waves also occur to a slightly lesser extent in B55.32.

References

[1] R. Baron, P. Boucaud, J. Carbonell, A. Deuzeman, V. Drach et al., *Light hadrons from lattice QCD with light (u,d), strange and charm dynamical quarks*, *JHEP* **1006** (2010) 111 [1004.5284].

[2] F. Zimmermann, *Oscillating Autocorrelation and the HMC Algorithm*, in *Proceedings of The 39th International Symposium on Lattice Field Theory — PoS(LATTICE2022)*, vol. 430, p. 045, 2023, DOI.

[3] E. Shuryak, I. Zahed, *Hadronic structure on the light front. I. Instanton effects and quark-antiquark effective potentials*, *Phys. Rev. D* **107** (2023) 034023 [2110.15927].

[4] S. Amoroso, D. Kar, M. Schott, *How to discover QCD Instantons at the LHC*, *Eur. Phys. J. C* **81** (2021) 624 [2012.09120].

[5] V.A. Khoze, V.V. Khoze, D.L. Milne, M.G. Ryskin, *Hunting for QCD instantons at the LHC in events with large rapidity gaps*, *Phys. Rev. D* **104** (2021) 054013 [2104.01861].

[6] F. Zimmermann, H. Forkel, M. Muller-Preussker, *Vacuum structure and string tension in Yang-Mills dimeron ensembles*, *Phys. Rev. D* **86** (2012) 094005 [1202.4381].

[7] K. Jansen, C. Urbach, *tmLQCD: A Program suite to simulate Wilson Twisted mass Lattice QCD*, *Comput.Phys.Commun.* **180** (2009) 2717 [0905.3331].

[8] C. Alexandrou, A. Athenodorou, K. Cichy, A. Dromard, E. Garcia-Ramos, K. Jansen et al., *Comparison of topological charge definitions in Lattice QCD*, *Eur. Phys. J. C* **80** (2020) 424 [1708.00696].

[9] S.O. Bilson-Thompson, D.B. Leinweber, A.G. Williams, *Highly improved lattice field strength tensor*, *Annals Phys.* **304** (2003) 1 [hep-lat/0203008].

[10] F. Bruckmann, F. Gruber, K. Jansen, M. Marinkovic, C. Urbach, M. Wagner, *Comparing topological charge definitions using topology fixing actions*, *Eur. Phys. J. A* **43** (2010) 303 [0905.2849].

[11] M. Campostrini, A. Di Giacomo, H. Panagopoulos, *The topological susceptibility on the lattice*, *Physics Letters B* **212** (1988) 206.

[12] A. Athenodorou, P. Boucaud, F. De Soto, J. Rodríguez-Quintero, S. Zafeiropoulos, *Instanton liquid properties from lattice QCD*, *JHEP* **02** (2018) 140 [1801.10155].

[13] F. Cuteri, *QCD thermodynamics: an overview of recent progress*, vol. 430, p. 243, 2023, DOI.

[14] J. Lenz, L. Pannullo, M. Wagner, B. Wellegehausen, A. Wipf, *Inhomogeneous phases in the Gross-Neveu model in 1+1 dimensions at finite number of flavors*, *Phys. Rev. D* **101** (2020) 094512 [2004.00295].